processes

MDPI

Article

The Coal-Forming Environment at the End of the Late Permian and Its Control on Trace Elements: The Upper Xuanwei Formation in Eastern Yunnan, China

Juan Wang [1,2,3,*], Longyi Shao [2] and Xuetian Wang [2]

[1] School of Resources and Environment, Henan Polytechnic University, Jiaozuo 454003, China
[2] College of Geoscience and Surveying Engineering, China University of Mining and Technology, Beijing 100083, China; shaol@cumtb.edu.cn (L.S.); wxskyer@gmail.com (X.W.)
[3] Collaborative Innovation Center of Coal Work Safety and Clean High Efficiency Utilization, Henan Polytechnic University, Jiaozuo 454003, China
* Correspondence: wangjuan@hpu.edu.cn

Abstract: Forming environments have important effects on the dispersion and enrichment of trace elements in coal. The C_3 coal seam of the Xuanwei Formation in eastern Yunnan was used as a case study to reconstruct the peat-forming environment based on coal facies parameters and geochemical characteristics, and its influence on trace element (including rare earth elements and yttrium, REY) enrichment was investigated. The C_3 coal was classified as medium rank bituminous coal with an ultra-low moisture content, medium-high ash yield, and medium-low volatile content. Compared to the average values for Chinese coal, Cu and V were enriched and Co was slightly enriched in the C_3 coal. Compared with the average values for world coal, Cu and V were enriched while several other trace elements were slightly enriched in the C_3 coal, including Co, Hf, Nb, Sc, Ta, Zn, and Zr. The C_3 coal was deposited in the limno-telmatic environment with fresh water, and reducing conditions. Trace elements, including Cu, V, Hf, Nb, Sc, Ta, Zr, Zn, Co, and REY, were typically enriched in the limno-telmatic environment with fresh water and reducing conditions. Additionally, REY and V were also significantly enriched in brackish water limno-telmatic conditions with the same depositional environment.

Keywords: Late Permian coal; trace element geochemistry; coal facies; depositional environment; Xuanwei Formation

check for updates

Citation: Wang, J.; Shao, L.; Wang, X. The Coal-Forming Environment at the End of the Late Permian and Its Control on Trace Elements: The Upper Xuanwei Formation in Eastern Yunnan, China. *Processes* **2023**, *11*, 2936. https://doi.org/10.3390/pr11102936

Academic Editors: Junjian Zhang and Zhenzhi Wang

Received: 17 August 2023
Revised: 1 October 2023
Accepted: 3 October 2023
Published: 9 October 2023

1. Introduction

The Late Permian was the most important coal-forming period in South China and represents a critical turning period in geological history, during which a series of geological events occurred, culminating in the Permian-Triassic mass extinction [1]. As a product of the death and accumulation of paleoplants and special organic sedimentary rock, coal is an important carrier of paleoecological and paleoenvironmental information in geological history, containing records of the paleoclimate and paleoenvironmental information during the peat deposition period [2]. At the end of the Late Permian, Southwest China became a refuge for several paleophytic peat-forming plants due to its warmer and more humid climate than other regions [3], and the Late Permian coal seam developed. Therefore, this region has become an excellent area for studying paleoenvironmental changes during the Late Permian mass extinction period.

Several paleoenvironmental studies have conducted through geochemical analyses of the elemental contents in coal [4–6]. In the peatification stage, the types and amounts of trace elements in peatland lay the foundation for trace elements in coal, and in the subsequent coalification stage, although the types and amounts of trace elements continue to change, they tend to have significant effects only on a local scale [5,7–9]. Dai et al. [7]

suggested that Late Permian coals were affected by sediment-source region, multi-stage volcanic ash, and multi-stage hydrothermal fluid injections. However, the impact of the peatland environment on coal formation has not been considered. Coal facies contain different combinations of maceral components, and the study of coal facies mainly focuses on the sedimentary environment of coal formation, including coal-forming plants, redox conditions, water activity, pH value, and coal pore structure [10–16]. Minerals are the major hosts of the vast majority of elements present in coal, such as rare earth elements generally associated with clay minerals, while other trace elements are often associated with pyrite, clay minerals, and many other minerals [17,18]. Therefore, it is more convincing to reconstruct the paleoenvironment of the coal period by combining coal facies, mineral composition, and element geochemical parameters. In this study, Xuanwei County, one of the main coal-producing areas in Southwest China, was selected as the research area. We investigated the coal facies, mineralogy, and trace element geochemistry of the C_3 coal seam of the Lefeng mineat Xuanwei. Moreover, there are few reports on C_3 coal so far. To identify the cause of the large mass extinction, this study attempted to resconstruct the Late Permian coal-forming peatland environment using various pieces of geological evidence, especially the contents of toxic and harmful heavy metals in the original environment.

2. Geological Setting

During the Late Permian, the study area of Xuanwei County in eastern Yunnan Province was part of the western margin of the South China Plate, with an equatorial paleolatitude (Figure 1a) [19]. Siliciclastic sediments in this area were supplied predominantly from the Khangdian Oldland to the west. This is a large area of ancient crystalline rocks reduced to a low relief by lengthy erosion through the Late Paleozoic, which was significantly affected by Emeishan mantle plume activity [19–21]. Controlled by transgressions from the east throughout the Late Permian, the depositional environments in eastern Yunnan and western Guizhou vary from marine, transitional, to terrestrial facies from east to west (Figure 1b) [19]. The Xuanwei Formation consists mainly of fine-grained sandstone, siltstone, and shale, with some parting beds and numerous coal seams, including the C_3 coal seam, which is dominated by terrestrial fluvial facies [19,22]. The Xuanwei Formation unconformably overlies Emeishan basalt and is conformably overlain by the Kayitou Formation of the Lower Triassic (Figure 1c).

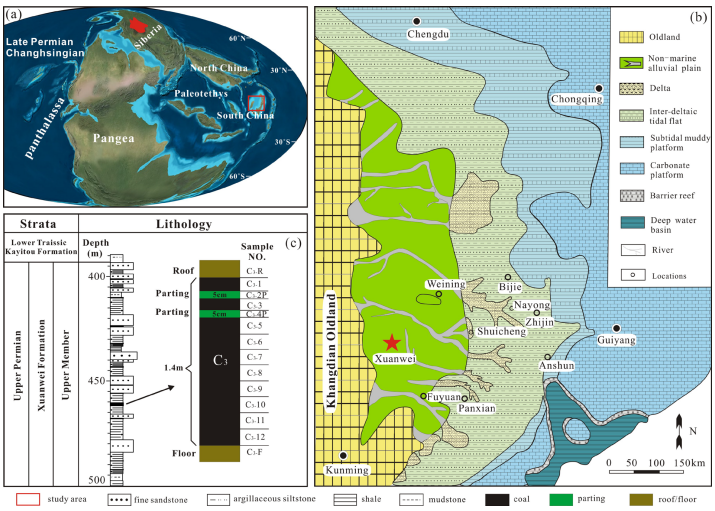

Figure 1. Location and geological context for the study area, including (**a**) Changhsingian (Late Permian) paleogeography showing the position of the South China Plate (modified from the ~252 Ma map of the webpage http://deeptimemaps.com/global-paleogeography-and-tectonics-in-deep-time, accessed on 10 July 2023); (**b**) Palaeogeography of southwestern China in the Changhsingian (Late Permian) (modified from Shao et al. [19]); (**c**) Lithology of the strata in Upper Member of Xuanwei Formation and horizons of samples in the C_3 coal seam of the Lefeng mine.

3. Materials and Methods

Samples were collected from the C_3 coal seam of the Late Permian Xuanwei Formation in the Lefeng mine, about 40 km NE of Xuanwei City, which is the main seam exploited and measures about 1.4 m in thickness with two tonstein layers, each approximately 5 cm thick (Figure 1c). A total of 14 samples, including 10 coal samples, 2 roof and floor samples, and 2 parting samples, were collected at approximately 10 cm vertical spacing intervals from top to bottom of the seam. The roof, floor, and partings were all mudstone. The mass of each sample collected was ≥2 kg and all samples were immediately stored in plastic bags to ensure as little contamination as possible.

The partial proximate analysis was conducted at the Chongqing Station of Coal Quality Supervision and Inspection according to ASTM D 3173-11, 3174-11, and 3175-11 (2011) [23–25]. Vitrinite reflectance and quantitative coal maceral statistics were determined at Henan Polytechnic University. Vitrinite reflectance was conducted under oil immersion at 500× magnification using a reflected light microscope (Axioskop 40, Zeiss, Jena, Germany) with an MSP UV-VIS 2000 microphotometer following the Chinese Standard GB/T 40485-2021 [26]. The standard reference for vitrinite reflectance determination was gadolinium gallium garnet with a calculated standard reflectance of 1.9702% for λ = 589 nm under oil immersion. Maceral constituents were identified using white light reflectance microscopy and more than 500 counts were measured for each polished pellet. Quantitative coal maceral statistics were determined using a polarizing microscope (Axioskop 40, Zeiss) according to the Chinese Standard GB/T 15588-2013 [27].

Trace and rare earth element (REE) analyses were performed at the Analytical Laboratory of Beijing Research Institute of Uranium Geology. The bulk samples were air-dried, crushed, ground to less than 200 mesh, and dried for 2 h in a drying oven at 105~110 °C. The samples were then preprocessed by low-temperature airproof acid digestion, the detailed procedure of which is described hereafter. An accurately weighed sample of 0.0500 g was mixed with 1 mL of HF, 3 mL of HNO_3, and 1 mL of $HClO_4$ in a dedicated 25 mL digestion vessel. After the cap assembly was sealed, the vessel was placed on a low-temperature electric warming plate for heating at 125 °C for 24 h. Finally, the residue was dissolved with 1% HNO_3 and then transferred to a 50 mL volumetric flask. The elemental composition of the prepared sample was then determined using inductively coupled-plasma mass spectrometry (ICP-MS) (ElEMENT, Finnigan MAT, Bremen, Germany) with a relative analysis error of ±5%, according to the Chinese Standard GB/T 14506.30-2010 [28]. The final results were reported as μg/g of coal on a dry basis for each sample.

The mineralogical composition of the roof, floor, partings, and coal samples were examined by scanning electron microscopy coupled with an energy dispersive X-ray analyzer (SEM-EDS) and powder X-ray diffraction (XRD). Samples were broken into small pieces first. Then, the fresh and smooth surfaces of samples were selected and coated with very thin layers of gold film. The micromorphology of minerals was observed and determined by SEM (JSM-6390 LV, JEOL, Tokyo, Japan) equipped with EDS (INCA ENERAGY 250, Bruker, Saarbrucken, Germany). Samples were crushed and ground to less than 200 mesh, then further subjected to low-temperature ashing (LTA) in an EMITECH K1050X Plasma Asher (Emitech, London, UK). Subsequently, the LTA ashes were analyzed by XRD (Bruker D8 Advance, Bruker, Saarbrucken, Germany). The XRD patterns were collected in the 2θ range of 5~90° using Cu Kα radiation. The SEM-EDS and XRD analyses of tonstein were carried out at the Analytical and Testing Center, Henan Polytechnic University.

4. Results

4.1. Partial Proximate Analysis and Vitrinite Reflectance

The vitrinite reflectance of the C_3 coal ranged from 1.05 to 1.77 with an average value of 1.33 (Table 1), indicating a bituminous coal according to the ASTM classification (ASTM D388-12, 2012) [29]. Coals with a moisture content of 0.84~1.49% are classified as ultra-low moisture coals according to the Chinese Standard MT/T850-2000 [30]. Coals with an ash

yield of 11.30~43.36% are considered medium-high ash coals according to the Chinese Standard GB/T 15224.1-2018 [31]. Coals with a volatile matter yield of 15.98~22.69% have medium-low volatile content according to the ASTM D388-12, 2012 [29].

Table 1. Partial proximate analysis and vitrinite random reflectance (%) of the C_3 coal.

Sample NO.	M_{ad}	A_d	V_d	F_{Cd}	R°_{ran}
C_3-1	0.84	54.39	11.77	33.84	1.21
C_3-3	1.04	56.93	11.97	31.1	1.32
C_3-5	1.05	27.01	18.66	54.33	1.05
C_3-6	1.12	11.3	22.69	66.01	1.15
C_3-7	1.02	12.81	21.21	65.98	1.23
C_3-8	1.47	24.3	19.11	56.59	1.35
C_3-9	1.36	22.62	19.69	57.69	1.22
C_3-10	1.49	43.36	15.98	40.66	1.77
C_3-11	0.88	24.17	19.78	56.05	1.77
C_3-12	1.41	19.55	20.98	59.47	1.26

M, moisture; A, ash yield; V, volatile matter; F_c, fixed carbon; ad, air-dry basis; d, dry basis; R^o_{ran}, random reflectance.

4.2. Maceral Composition

Table 2 summarizes the maceral and mineral data for 10 samples of the C_3 coal (typical coal macerals, see Figure 2). The samples typically contained little mineral matter (average 11.5%, range of 3.5~22.0%). They were predominantly vitrinite with a content of 72.6~94.0% (av. 83.2%), followed by inertinite with a content of 1.0~12.7% (av. 4.1%), whereas liptinite had only a very minor component with a content of 0~0.7% (av. 0.2%). The vitrinite mainly consist of collodetrinite (av. 36.1%) (Figure 2a), telocollinite (av. 22.5%) (Figure 2a), telinite (av. 12.9%) (Figure 2b), and vitrodetrinite (av. 11.8%). Within the inertinite, fusinite (Figure 2a,e) was the most abundant (av. 3.0%), followed by semifusinite (av. 0.7%) (Figure 2a,g), inertodetrinite (av. 0.4%) (Figure 2e), with minor amounts of macrinite (av. 0.1%) (Figure 2c) and sclerotinite (Figure 2d). The liptinite component was rarely developed (av. 0.2%), mainly cutinite and was only observed in a few samples due to its high degree of coalification (Figure 2f).

Table 2. Maceral composition, minerals and coal facies of the C_3 coal from the Lefeng mine (%).

Sample		C_3-1	C_3-3	C_3-5	C_3-6	C_3-7	C_3-8	C_3-9	C_3-10	C_3-11	C_3-12	Av.
Vitrinite	Telinite	11.2	8.2	13.7	5.6	18.7	23.6	16.7	20.6	6.8	3.7	12.9
	Collodetrinite	37.4	58.7	25.2	13.9	22.5	32.6	44.0	44.2	39.9	42.8	36.1
	Telocollinite	3.3	5.9	22.7	67.8	37.3	21.3	20.0	4.2	9.8	32.2	22.5
	Vitrodetrinite	20.7	12.8	18.1	6.7	12.6	8.9	6.0	10.9	11.9	9.3	11.8
	sub-total	72.6	85.6	79.7	94.0	91.1	86.4	86.7	79.9	68.4	88.0	83.2
Inertinite	Fusinite	9.5	1.1	0.8	2.3	4.4	1.1	0.8	0.7	7.6	1.2	3.0
	Semifusinite	2.3	0	0.2	0.2	0.7	0.6	0.2	0	1.8	0.7	0.7
	Inertodetrinite	0.9	0.8	0	0	0.3	0.2	0.4	0.2	0.2	0.7	0.4
	Macrinite	0	0	0	0	0	0	0	0.2	0	0.4	0.1
	Sclerotinite	0	0	0	0	0	0	0	0.2	0	0	0.0
	sub-total	12.7	1.9	1.0	2.5	5.4	1.9	1.4	1.3	9.6	3.0	4.1

Table 2. *Cont.*

Sample		C_3-1	C_3-3	C_3-5	C_3-6	C_3-7	C_3-8	C_3-9	C_3-10	C_3-11	C_3-12	Av.
Liptinite	Cutinite	0	0	0.2	0	0	0.7	0.6	0.4	0	0.4	0.2
Mineral matter	Clay minerals	1.6	2.9	5.0	0.9	0.5	2.3	1.0	3.4	0.7	0.9	1.9
	Quartz	11.1	7.1	13.1	0.2	1.2	7.2	8.4	4.2	20.3	7.0	8.0
	Pyrite	1.2	0.4	0	0.8	0.3	1.1	1.1	0.4	0.5	0.2	0.6
	Calcite	0.9	2.1	1.0	1.6	1.5	0.4	0.8	0.4	0.5	0.5	1.0
	Total	14.8	12.5	19.1	3.5	3.5	11.0	11.3	8.4	22.0	8.6	11.5
Coal facies	GI	5.72	45.11	79.70	37.60	16.87	45.47	61.93	11.68	7.13	34.00	—
	TPI	0.45	0.21	0.86	3.68	1.73	1.12	0.75	0.46	0.50	0.71	—

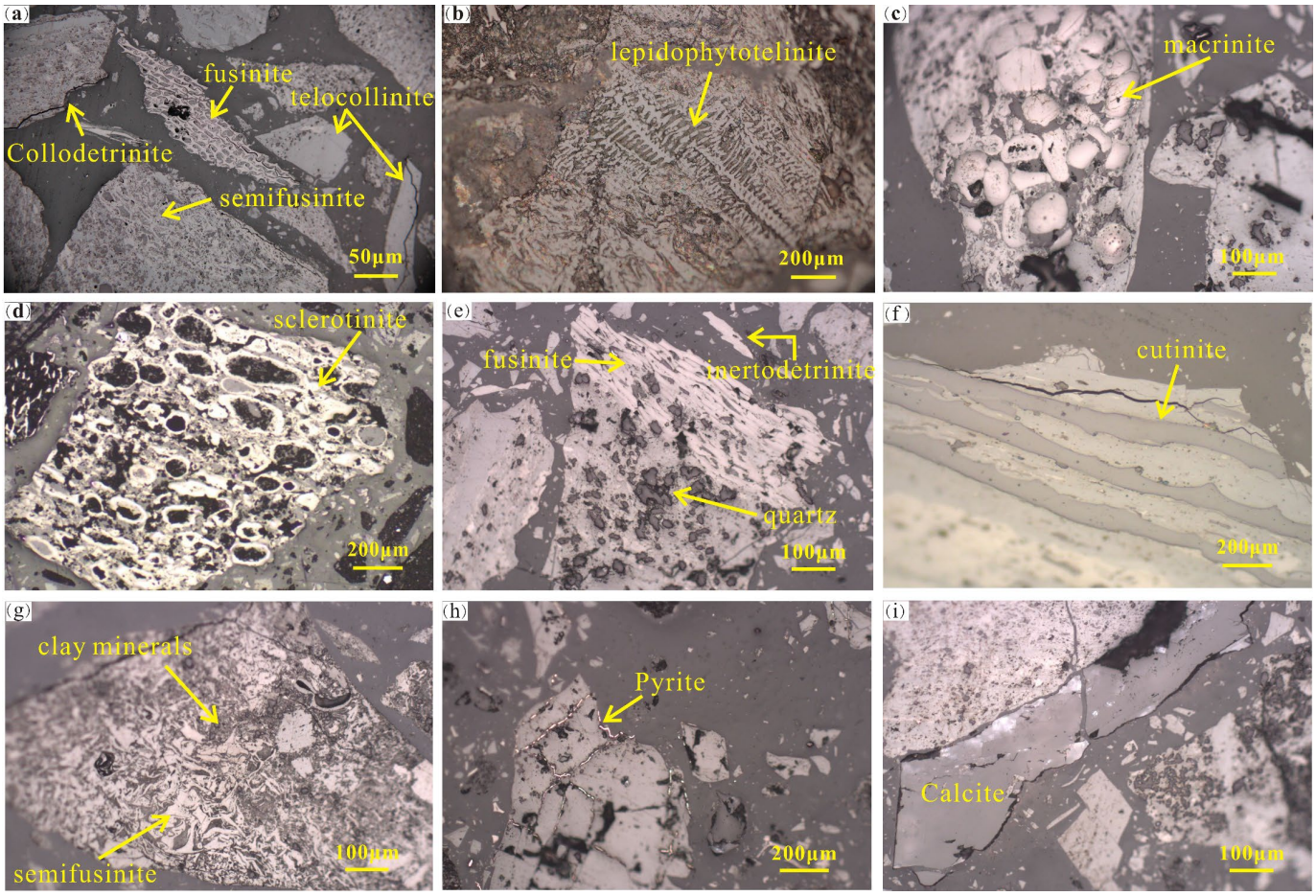

Figure 2. Maceral composition of the C_3 coal from the Lefeng mine (dry objective, reflected light). (a) collodetrinite, telocollinite, fusinite, and semifusinite. (**b**) lepidophytotelinite. (**c**) macrinite. (**d**) sclerotinite. (**e**) fusinite, inertodetrinite, and quartz. (**f**) cutinite. (**g**) clay minerals and semifusinite. (**h**) vein pyrite. (**i**) calcite.

The average content of the mineral matter in the maceral composition of the C_3 coal was 11.5% and was dominated by quartz (range 0.2~20.3%, av. 8.0%), followed by clay minerals (range 0.5~5.0%, av. 1.9%), calcite (range 0.4~2.1%, av. 1.0%), and pyrite (range 0~1.2%, av. 0.6%). Quartz was the most abundant mineral and was mostly embedded in collodetrinite or occurred as the cell lumen fillings of fusinite- and semifusinite (Figure 2e). Clay minerals typically occurred as dissemination with fine particles (Figure 2g) and were filled in the cell lumen of fusinite and semifusinite. Pyrite usually occurred as fracture filling (Figure 2h) or was scattered in collodetrinite. Calcite was distributed independently in bands or filled in the cell lumen of fusinite (Figure 2i).

4.3. Trace Elements in Coal

Table 3 shows the contents of trace and rare earth elements and yttrium (REY) in the C_3 coal, as well as a comparison with average levels in Chinese and world coals (μg/g). The concentration coefficient (CC, CC = element content in sample/average element content in Chinese or world coal) proposed by Dai et al. [32] was used to evaluate the dispersion and enrichment of trace elements in the C_3 coal, with categories of: $10 < CC < 100$, significantly enriched; $5 < CC < 10$, enriched; $2 < CC < 5$, slightly enriched; $0.5 < CC < 2$, normal; $CC < 0.5$, depleted. In comparison to Chinese coal, Cu and V were enriched in the C_3 coal, Co was slightly enriched, and Ba, Sr, and Tl were depleted; all other elements were normal. Compared with world coal, Cu and V were enriched, Co, Hf, Nb, Sc, Ta, Zn, and Zr were slightly enriched, and Ba, Rb, Sr, and Tl were depleted; all other elements were normal (Figure 3).

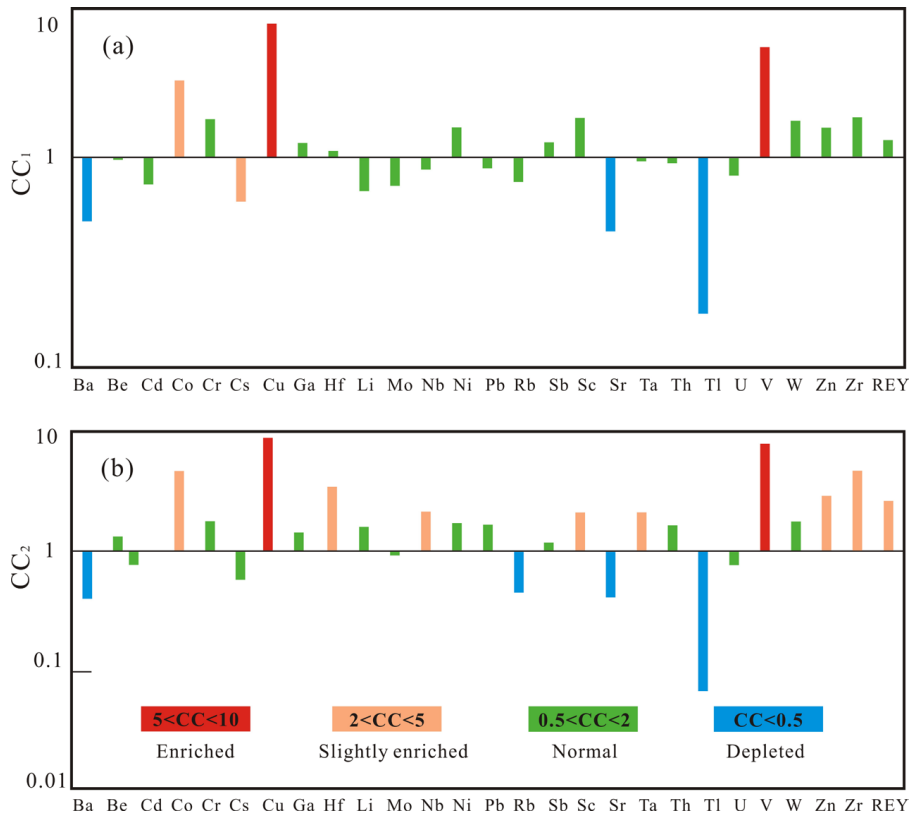

Figure 3. REY concentration coefficients of the C_3 coal from the Lefeng mine. (**a**) the concentration coefficient based on the Chinese coal; (**b**) the concentration coefficient based on the world coal.

Table 3. Contents of trace elements and REY of the C_3 coal from the Lefeng mine (μg/g).

Sample	C_3-1	C_3-3	C_3-5	C_3-6	C_3-7	C_3-8	C_3-9	C_3-10	C_3-11	C_3-12	Av.	China [32]	World [33]	CC_1	CC_2
Ba	65.8	90.7	57.3	26.4	29.1	38.4	41.1	173	46	26.70	59.45	159	150	0.37	0.40
Be	0.587	1.65	1.9	1.38	1.42	2.03	1.96	5.92	2.34	1.85	2.10	2.11	1.6	1.00	1.31
Cd	0.532	0.104	0.086	0	0.082	0.194	0.115	0.109	0.328	0.11	0.17	0.25	0.22	0.66	0.75
Co	22.7	16.3	18.2	22.6	22.3	24.7	26.8	19.8	35.4	28.40	23.72	7.08	5.1	3.35	4.65
Cr	33.9	31.9	17.7	15.1	16.1	22.4	25.2	73.1	25.7	21.30	28.24	15.4	16	1.83	1.77
Cs	0.513	2.3	0.401	0.043	0.108	0.302	0.255	1.46	0.196	0.15	0.57	1.13	1	0.51	0.57
Cu	69.3	116	44.5	34.4	45.7	166	117	594	83	143.00	141.29	17.5	16	8.07	8.83
Ga	5.72	11.1	9.13	3.62	4.31	9.58	7.27	20.4	5.63	5.87	8.26	6.55	5.8	1.26	1.42
Hf	2.65	3.64	5.27	1.14	1.7	4.52	3.84	14.1	2.37	2.14	4.14	3.71	1.2	1.12	3.45
Li	7.44	19.3	23.4	6.68	8.99	20.5	14.5	72.8	7.96	8.22	18.98	31.8	12	0.60	1.58
Mo	0.585	1.37	1.12	0.371	0.556	1.23	2.43	8.91	0.502	2.96	2.00	3.08	2.2	0.65	0.91
Nb	7.96	7.93	6.84	2.21	2.85	6.2	6.7	29	5.59	3.65	7.89	9.44	3.7	0.84	2.13
Ni	23.2	16.7	17.3	20	18.9	25.5	21.4	29.7	24.3	24.00	22.10	13.7	13	1.61	1.70
Pb	9.74	8.26	21.8	16.7	10.1	17.2	13.3	10.2	10.1	11.30	12.87	15.1	7.8	0.85	1.65
Rb	6.75	16.1	5.02	1.53	1.83	3.47	3.47	20.7	2.98	1.93	6.38	9.25	14	0.69	0.46
Sb	1.27	1.24	0.728	0.956	0.894	0.877	0.844	2.11	0.772	1.04	1.07	0.84	0.92	1.28	1.17
Sc	5.81	7.49	7.01	2.12	3.78	9.42	8.38	25.5	5.47	6.91	8.19	4.38	3.9	1.87	2.10
Sr	32.7	59.4	30.4	26.5	39.9	31.1	47	92	32.8	54.40	44.62	140	110	0.32	0.41
Ta	0.397	0.536	0.603	0.131	0.212	0.542	0.48	2.32	0.394	0.26	0.59	0.62	0.28	0.95	2.10
Th	2.01	7.93	7.93	1.11	1.9	6.64	4.68	16.8	2.59	2.32	5.39	5.84	3.3	0.92	1.63
Tl	0.04	0.071	0.027	0.05	0.005	0.027	0.029	0.106	0.023	0.04	0.04	0.47	0.63	0.09	0.07
U	0.993	3.37	2.41	0.491	0.715	1.86	1.77	4.45	1.05	1.08	1.82	2.43	2.4	0.75	0.76
V	135	384	135	59.4	57.1	173	193	467	199	166.00	196.85	35.1	25	5.61	7.87
W	4.79	2.89	0.801	0.798	1.07	0.543	2.49	1.48	3.05	1.41	1.93	1.08	1.1	1.79	1.76
Zn	109	43.7	52.7	51.6	56.8	68.3	56.8	72.1	91.3	61.70	66.40	41.4	23	1.60	2.89
Zr	164	166	220	44	64.6	167	150	521	110	82.50	168.91	89.5	36	1.89	4.69
La	22.80	52.60	27.40	4.48	12.10	31.10	29.80	85.5	25.50	16.90	30.82	22.5	11	1.37	2.80
Ce	50.00	99.10	55.40	7.22	27.60	58.10	55.00	146	48.30	31.70	57.84	46.7	23	1.24	2.51
Pr	5.93	12.80	6.65	0.84	3.54	7.39	7.59	19.1	6.28	4.23	7.44	6.42	3.5	1.16	2.12
Nd	22.90	47.70	25.20	3.50	15.20	31.10	31.20	78.3	26.80	18.20	30.01	22.3	12	1.35	2.50
Sm	4.16	9.16	4.82	0.85	3.16	6.18	5.81	14.3	4.74	4.00	5.72	4.07	2.0	1.40	2.86
Eu	0.84	1.74	1.05	0.20	0.69	1.34	1.56	3.39	1.38	1.03	1.32	0.84	0.47	1.57	2.81
Gd	3.23	8.63	5.42	0.95	2.62	4.92	5.20	11.1	4.58	3.82	5.05	4.65	2.7	1.09	1.87
Tb	0.51	1.64	1.07	0.20	0.44	0.87	0.90	2	0.83	0.69	0.92	0.62	0.32	1.48	2.86
Dy	2.52	8.47	6.50	1.43	2.36	4.80	4.65	11.5	4.35	3.85	5.04	3.74	2.1	1.35	2.40
Y	11.00	49.30	46.00	11.2	13.2	24.7	22.7	55.3	25.4	19.1	27.79	18.2	8.4	1.53	3.31
Ho	0.45	1.62	1.47	0.32	0.43	0.82	0.85	2.18	0.83	0.64	0.96	0.96	0.54	1.00	1.78
Er	1.22	4.69	4.40	0.99	1.25	2.48	2.22	5.94	2.26	1.56	2.70	1.79	0.93	1.51	2.90
Tm	0.21	0.82	0.72	0.16	0.21	0.38	0.28	0.92	0.37	0.26	0.43	0.64	0.31	0.68	1.40
Yb	1.44	4.98	4.62	0.91	1.29	2.47	2.03	5.85	1.97	1.47	2.70	2.08	1.0	1.30	2.70
Lu	0.22	0.80	0.74	0.13	0.18	0.33	0.36	0.92	0.36	0.25	0.43	0.38	0.20	1.13	2.15
∑REY	127.43	304.05	191.46	33.38	84.26	176.98	170.15	442.30	153.95	107.70	179.17	135.89	68.47	1.32	2.62
K_2O [c]	0.313	0.395	0.127	0.027	0.044	0.087	0.098	0.607	0.081	0.052	—	—	—	—	—

CC_1 = element content in sample/element average content in Chinese coal; CC_2 = element content in sample/element average content in world coal; REY = La+Ce+Pr+Nd+Sm+Eu+Gd+Tb+Dy+Y+Ho+Er+Tm+Yb+Lu. [c] data for K_2O(%) cited from Wang [34].

4.4. REY in Coal

The REY content in coal was determined by dividing the materials into light, medium, and heavy fractions: LREY (La, Ce, Pr, Nd, and Sm), MREY (Eu, Gd, Tb, Dy, and Y), and HREY (Ho, Er, Tm, Yb, and Lu) [35]. The total REY content (ΣREY) in the C_3 coal was in the range of 33.38~442.30 μg/g (av. 179.17 μg/g) (Table 3), which was similar to that in Chinese coal (135.89 μg/g) [36], and slightly higher than that in world coal (68.47 μg/g) [33]. When values of La, Sm, Gd, and Lu were normalized to chondrites [37] (Table 4), REY could be identified as three enrichment types: L-type (light-REY; $La_N/Lu_N > 1$), M-type (medium-REY; $La_N/Sm_N < 1$, $Gd_N/Lu_N > 1$), and H-type (heavy-REY; $La_N/Lu_N < 1$) [35]. The REY enrichment patterns in the bench samples of the C_3 coal were all L-type.

Table 4. Geochemical parameters of REY in the C_3 coal from the Lefeng mine (in μg/g).

Sample	La_N	Sm_N	Gd_N	Lu_N	Eu_N	Ce_N	Pr_N	δ_{Eu}	δCe	δCe_{anom}
C_3-1	71.25	20.80	10.42	7.06	11.47	53.19	49.42	0.78	0.90	−0.013
C_3-3	164.38	45.80	27.84	25.90	23.84	105.43	106.67	0.67	0.80	−0.065
C_3-5	85.63	24.10	17.48	23.74	14.38	58.94	55.42	0.70	0.86	−0.036
C_3-6	14.00	4.27	3.06	4.26	2.70	7.68	7.03	0.75	0.77	−0.114
C_3-7	37.81	15.80	8.45	5.94	9.38	29.36	29.50	0.81	0.88	−0.031
C_3-8	97.19	30.90	15.87	10.65	18.36	61.81	61.58	0.83	0.90	−0.082
C_3-9	93.13	29.05	16.77	11.68	21.37	58.51	63.25	0.97	0.76	−0.094
C_3-10	267.19	71.50	35.81	29.74	46.44	155.32	159.17	0.92	0.75	−0.109
C_3-11	79.69	23.70	14.77	11.65	18.90	51.38	52.33	1.01	0.80	−0.084
C_3-12	52.81	20.00	12.32	7.97	14.11	33.72	35.25	0.90	0.78	−0.091

Chondritic values by A.G. Herrmann were used for normalization with the modification of REEs [35].

4.5. Minerals in Coal

The mineralogical composition of the partial samples from the C_3 coal seam were examined by XRD and SEM-EDX. The XRD results (Figure 4) showed that kaolinite was the dominant mineral in the partings, roof, and floor, followed by quartz. The roof and floor also contained certain amounts of anatase and halite. Additionally, some calcite, pyrite, gypsum, barite, and montmorillonite were identified in the coal samples using SEM-EDX (Figure 5). Kaolinite occurred in the form of "accordion" aggregates in partings C_3-2 and C_3-4, respectively. Pyrite and calcite often occurred as veins in the C_3 coal. Gypsum occurred as a plate-like morphology, while barite often occurred as films in the C_3 coal. Montmorillonite showed a typical honeycomb morphology, which only appeared in the roof of the C_3 coal seam.

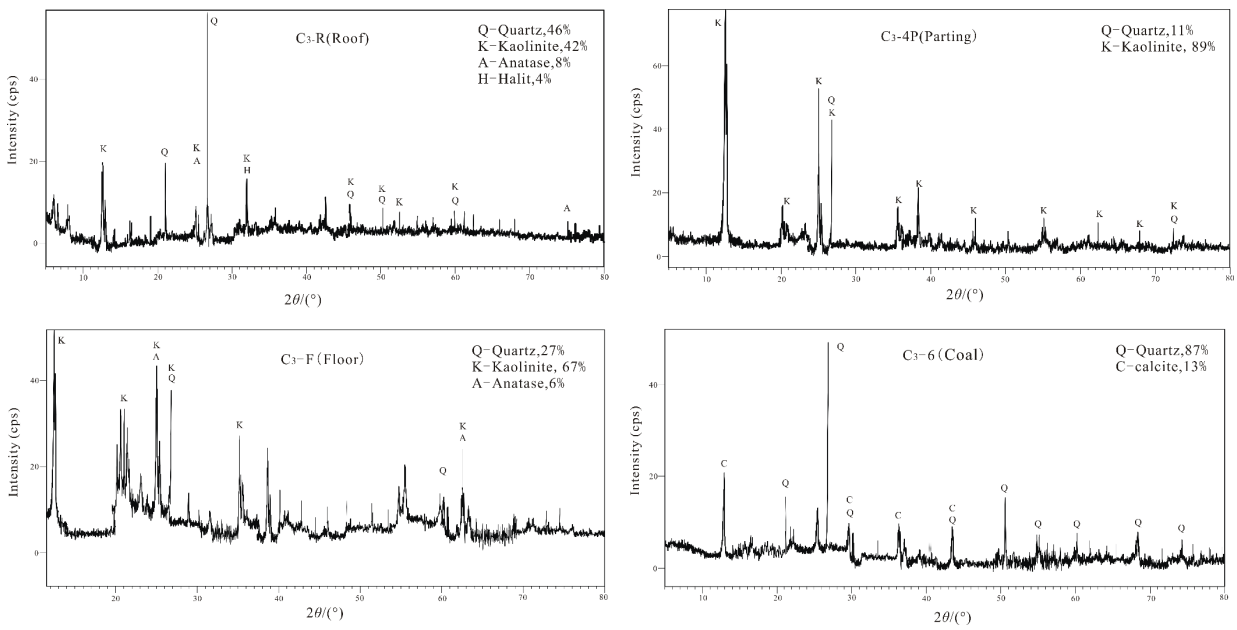

Figure 4. XRD patterns of samples from the C_3 coal seam.

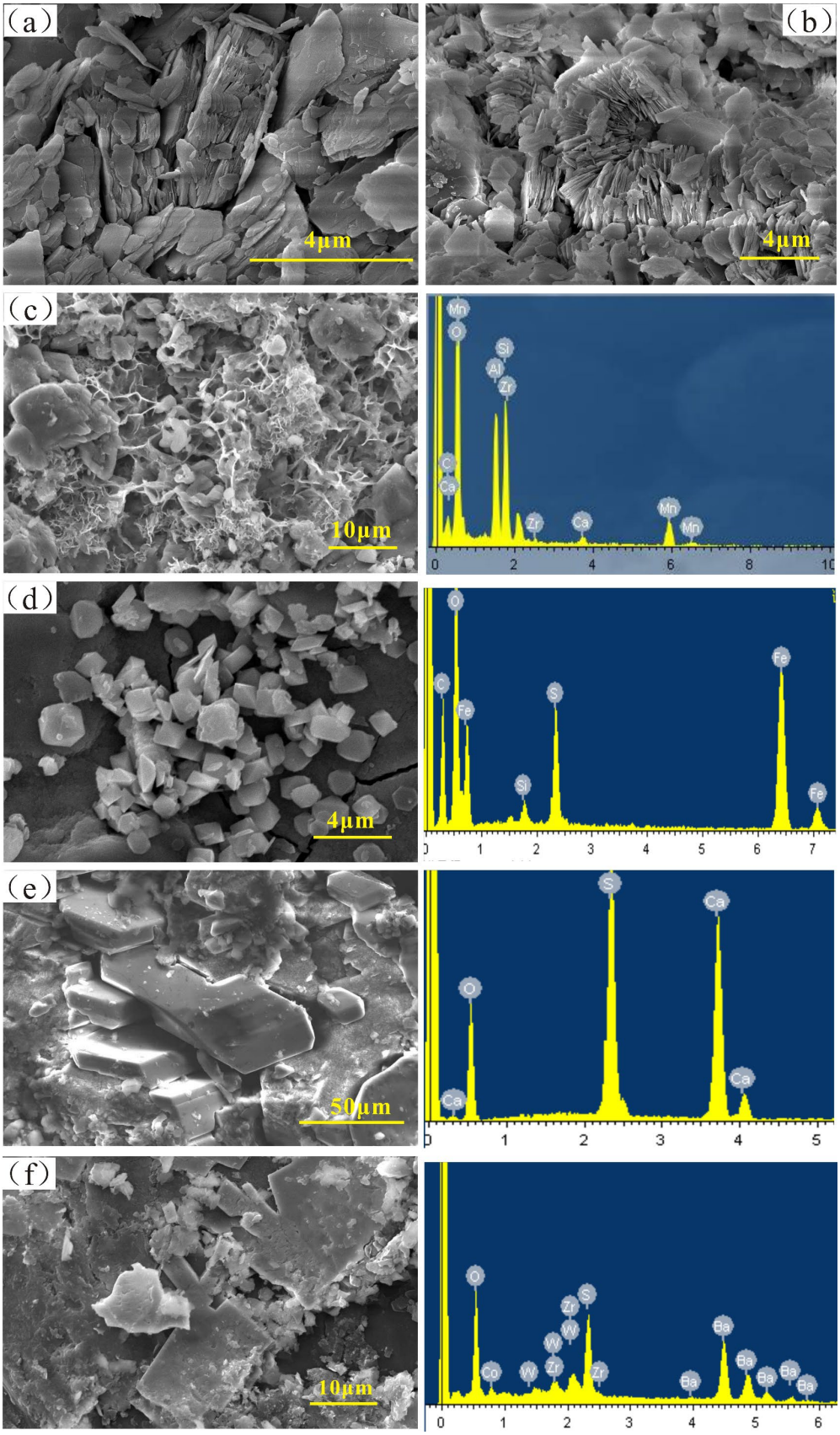

Figure 5. SEM-EDS results of samples from the C_3 coal seam: (**a**,**b**) kaolinite in partings C_3-2 and C_3-4; (**c**) montmorillonite in roof; (**d**) pyrite in coal; (**e**) gypsum in coal; (**f**) barite in coal.

5. Discussion

The accumulation and distribution of trace elements in coal can be controlled by numerous factors during peatification and coalification as well as the weathering and oxidation processes that occur after coal formation [38,39]. The types and amounts of trace elements in coal have already been well established during the peatification stage, and migration and transformation during the later coalification stage usually only occur locally. It is therefore particularly important to study the distribution of trace elements in the peatification stage [4,5,38,40,41].

5.1. Provenance Characteristics

REY and some trace elements, including Zr, Sc, Co, Th, and Hf, have excellent stability during weathering, transport, deposition, and compaction to rock, and can therefore represent the elemental characteristics of provenance. The contents and ratios of these stable elements are commonly used to identify the source materials of rocks.

Diagrams of $\sum$REE-$(La/Yb)_N$ and La/Sc-Co/Th were constructed to analyze the source rocks. In Figure 6a, samples including coals, partings, and the seam roof were predominantly plotted in the basalt area, with the exception of C_3-F. Partings in the C_3 seam were classified as felsic volcanic rocks in the La/Sc-Co/Th diagram, the seam roof and floor originated from andesite rock, whereas the coal was plotted in the basalt and andesite area (Figure 6b). From the dispersion of the samples plotted in these two diagrams, it was inferred that the Late Permian coal-forming materials were related to intermediate-basic volcanic rock.

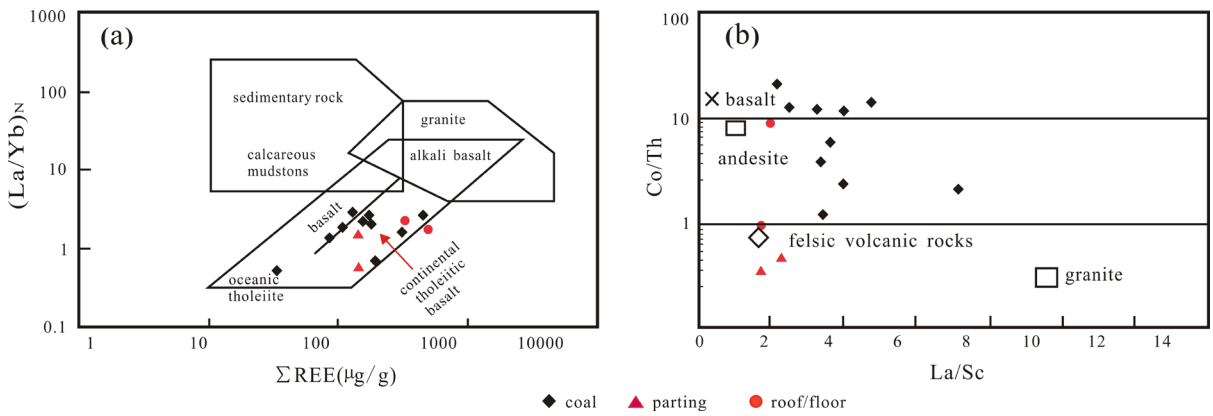

Figure 6. Source rock discrimination diagrams of the Xuanwei Formation coal measures. (**a**) Diagram of $\sum$REE-$(La/Yb)_N$ (modified from Roser et al. [42]); (**b**) Diagram of La/Sc-Co/Th (modified from McLennan et al. [43]).

Moreover, the accordion texture of kaolinite aggregates in partings C_3-2 and C_3-4 is often interpreted as volcanogenic in origin [36]. This conclusion was in accordance with that of a previous study that found Emeishan basalt and its weathering alteration products were the only terrigenous material supply in eastern Yunnan [7]. It is worth noting that vein pyrite and thin film barite were determined in most C_3 coal samples, so it was inferred that there were low-intermediate temperature hydrothermal activities after coal formation, which may also have contributed to the enrichment of trace elements in the C_3 coal.

5.2. The Depositional Environment

5.2.1. Coal Facies Interpretation

Coal facies play a significant role in reconstructing the material conditions and depositional environments of coal-forming periods [39]. Coal facies parameters, including the Gelation Index (GI), Texture Preservation Index (TPI), Groundwater Flow Index (GWI), Vegetation Index (VI), and Vitrinite content/Inertinite content (V/I), are widely used to

evaluate depositional environment-related conditions, i.e., coal-forming plants, swamp medium conditions, and hydrodynamic conditions [10,11].

The GI refers to the ratio of macerals in a wet environment (vitrinite) to that in a dry environment (inertinite). A high GI value indicates a wetter coal-forming environment and deeper water cover [44]. The TPI reflects the degree of preservation and degradation, and the higher the TPI value, the better the preservation degree of plant cells, which can be used to determine the type of coal-forming plant [14,45]. The GI and TPI indexes are modified based on Diessel [11] and Jiu et al. [46] as follows:

GI = (Total Vitrinite + Macrinite)/(Fusinite + Semifusinite + Inertodetrinite)

TPI = (Telinite + Telocollinite + Fusinite + Semifusinite)/(Collodetrinite + Macrinite + Inertodetrinite + Vitrodetrinite)

These two coal facies parameters were calculated for the C_3 coals and the results are presented in Table 2. Cross-plots of TPI-GI-based coal facies parameters are shown in Figure 7. In the TPI-GI cross-plot, the C_3 coal was distributed in both limno-telmatic and humid forest swamp areas, indicating that the Late Permian C_3 coal was formed in a low-lying peat swamp. More specifically, the early and late peat stages were in limno-telmatic conditions; however, the middle peat stage evolved into humid forest swamp. It can be indicated that the C3 coal formed in a wet low peat swamp dominated by herbaceous plants that gradually evolved into a forest swamp.

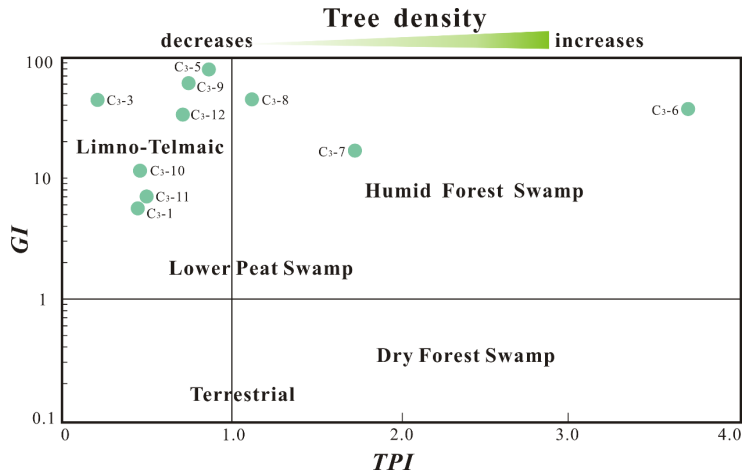

Figure 7. TPI-GI coal facies of the C_3 coal from the Lefeng mine (modified from Diessel [13]).

5.2.2. Trace Element Analysis

The Sr/Ba ratio is the most commonly used geochemical parameter for paleosalinity analysis. However, the frequent occurrence of barites (Figure 5f) suggested more than normal barium content in the C_3 coal seam, and thus the Sr/Ba ratio may indicate an inaccurate paleosalinity.

Rb/K ratio is also used to indicate the paleosalinity [47]. The potassium (K) abundance has an intimate relationship with the illite content. Given the similar ionic radius between K and rubidium (Rb), K can be easily replaced by Rb in illite [48]. Given an increased salinity, more Rb is absorbed into the clay minerals [49]. Therefore, the higher the salinity, the stronger the Rb adsorption and the higher the Rb/K ratio. Since the Rb and K contents are not of the same order of magnitude, the Rb value is expanded by 1000 times to indicate the paleosalinity: >6 for salt water, 4~6 for brackish water, and <4 for freshwater [47,50]. The 1000 Rb/K_2O ratio values of the C_3 coal ranged from 2.16 to 5.67 (av. 3.83) (Table 3), indicating a mostly freshwater body.

The V/(V+Ni) ratio in sedimentary rocks is often used as a geochemical indicator of redox sensitivity. The hypervalent ions of V can be reduced and enriched in an anoxic environment, while Ni is mainly enriched in a sulfate-reducing environment. This difference can distinguish the degree of redox in a sedimentary environment [51]. Hatch and

Leventhal [52] proposed that V/(V+Ni) ratio values of <0.46, 0.46~0.60, 0.60~0.84, and >0.84 indicate strong oxidizing, oxidizing, anoxic reducing, and euxinic reducing environments, respectively. The V/(V+Ni) ratio values of the C_3 coal ranged from 0.75 to 0.96 (av. 0.87), which indicated that the coal-forming swamp had a stable reducing environment.

Rare earth elements (REEs) are often used to indicate the redox conditions of the paleoenvironment due to their sensitivity to changes in the sedimentary environment. The Ce anomaly parameter (Ce_{anom}) proposed by Elderfield et al. has been widely used in the identification of paleoredox conditions [53,54]. Generally, $Ce_{anom} > -0.1$ indicates a reducing environment, while $Ce_{anom} < -0.1$ indicates an oxidizing environment. The Ce_{anom} values of the C_3 coal varied from −0.114 to −0.013 (av. −0.072), except for C_3-6 and C_3-10, indicating a reducing environment. Combined with the V/(V+Ni) ratios, it was concluded that the C_3 coal was mainly deposited in a reducing environment.

5.3. Influence of Depositional Environment on Enrichment of Trace Elements

In addition to the influence of ancient plants and detrite material, the depositional environment-related conditions of peat swamps, including the oxidation–reduction state, pH value, paleosalinity, hydrodynamic conditions, and paleoclimate, play an important role in the enrichment of trace elements in coal [40,41]. The relationship between the depositional environment of peat swamps and the content of trace elements was obtained by normalizing the trace element contents in the coal bench samples (Figure 8). Compared to the average contents of Chinese and world coals, Cu and V were enriched and some trace elements were slightly enriched in the Lefeng mine coal, including Co, Hf, Nb, Sc, Ta, Zn, Zr, and REY. Most of the elements, including Cu, V, Hf, Nb, Sc, Ta, Zr, and REY, were concentrated in sample C_3-10, which represented a limno-telmatic environment with freshwater and reducing conditions (Figure 8). Moreover, REY and V were also significantly enriched in the limno-telmatic environment with brackish water and reducing conditions of sample C_3-3. However, REE may also be affected by volcanic ash input, so the cause of REE enrichment is more complicated. Only Zn and Co were enriched in bench sample C_3-11, which were originated from a depositional environment consistent with C_3-10.

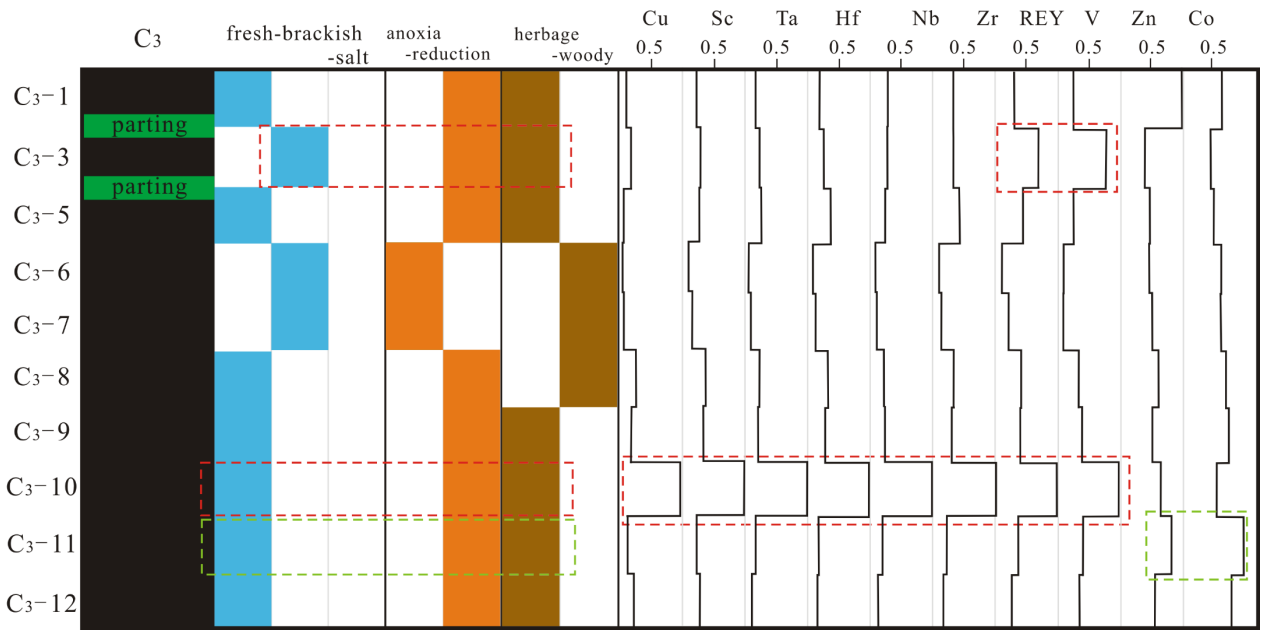

Figure 8. Relationship between paleo-peat environment and trace elements of the C_3 coal from the Lefeng mine. The position of the color blocks corresponds to the meaning of the title at the top of the figure, and the line represent the content distribution of the elements after normalization.

Since the ash yields of bench samples C_3-3 and C_3-10 were 56.93% and 43.36%, respectively (Table 1), the correlation coefficients between Cu, V, Hf, Nb, Sc, Ta, Zr, and REY enrichment in the two samples and ash yield were calculated (Figure 9). Only V and REY were significantly correlated with ash yield (confidence level of 90%), while the other elements were only weakly correlated with ash yield. Therefore, it was concluded that the enrichment of these elements in the two samples was not caused by a high ash content, which meant that these elements were not present in the minerals but occurred in other forms. The REY and V contents were locally enriched in the same horizon, and Wang et al. [55] also suggested that V was significantly correlated with REEs. The solubility of REEs in rivers is very low, and they usually react with unsaturated groups such as OH- and COOH- in the +3 oxidation state to form stable rare earth complexes and then migrate. When river water mixes with seawater, large amounts of the $Al(OH)_3$ colloid in the transporting medium will polymerize, resulting in rapid precipitation and enrichment of REEs. It was concluded that the enrichment of REEs was related not only to the ash yield but also to the brackish water environment caused by transgression. Ren et al. [38] also argued that peat swamps affected by seawater were more likely to enrich V than the coal affected by fresh water. In addition, the enrichment of these two elements did not exclude the influence of volcanic ash input.

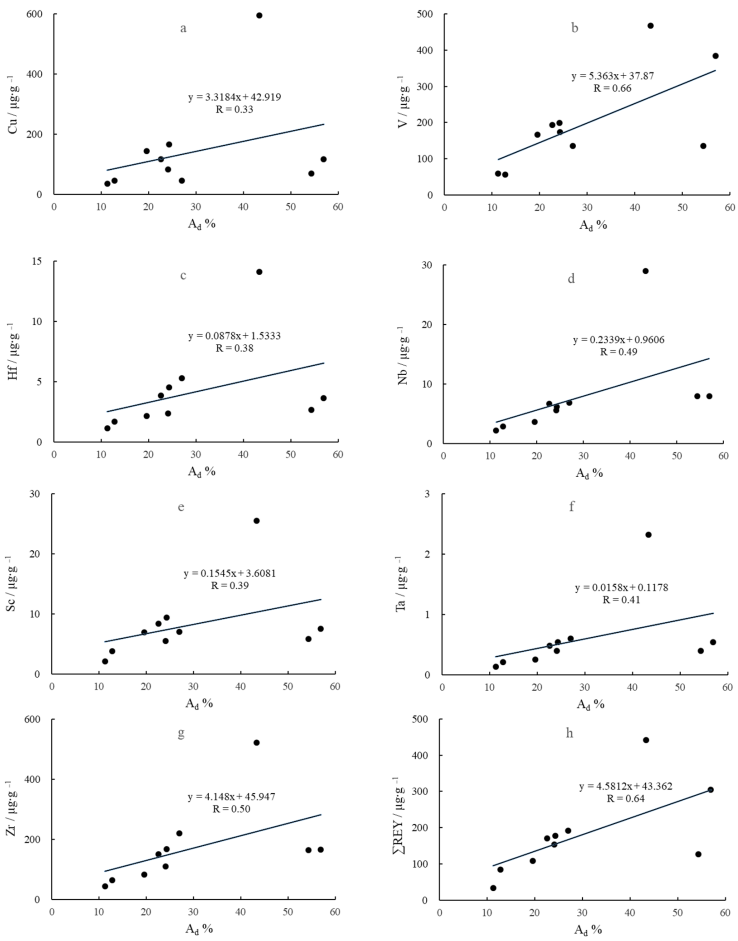

Figure 9. Correlation coefficients (*R*) between trace elements and ash content of the C_3 coal from the Lefeng mine. (**a**) correlation coefficient between Cu and ash content. (**b**) correlation coefficient between V and ash content. (**c**) correlation coefficient between Hf and ash content. (**d**) correlation coefficient between Nb and ash content. (**e**) correlation coefficient between Sc and ash content. (**f**) correlation coefficient between Ta and ash content. (**g**) correlation coefficient between Zr and ash content. (**h**) correlation coefficient between ∑REY and ash content.

Among these enriched trace elements, Cu and V, which were the most enriched, are essential elements for the human body, but excessive amounts can lead to toxic reactions. The enrichment of these two elements in peat swamps at that time may be one of the causes of mass extinction at the end of the Late Permian. Other enriched elements have no known harmful effects on the environment.

6. Conclusions

The peat swamp depositional environment of the C_3 coal in the Late Permian Xuanwei Formation in eastern Yunnan was reconstructed using coal facies parameters together with geochemical characteristics, and the influence of the depositional environment on trace element (including REY) enrichment was investigated. The conclusions are as follows.

(1) The C_3 coal was classified as a bituminous coal with an ultra-low moisture content, a medium-high ash yield, and medium-low volatile content. Compared with the average values for Chinese and world coals, Cu (av. 141.29 μg/g) and V (av. 196.85 μg/g) were enriched, while several other trace elements were slightly enriched, including Co, Hf, Nb, Sc, Ta, Zn, and Zr in the C_3 coal.
(2) The C_3 coal was deposited in a low-lying peat swamp typied by fresh water, and reducing conditions, mainly within a limno-telmatic environment.
(3) Trace elements, including Cu, V, Hf, Nb, Sc, Ta, Zr, Zn, Co, and REY, were easily enriched in the limno-telmatic environment with fresh water and reducing conditions. Additionally, REY and V were also significantly enriched in the brackish water limno-telmatic conditions with the same depositional environment.

As the coal seam closest to the mass extinction period at the end of the Late Permian, their geochemical and mineralogical characteristics can reflect the paleoenvironmental changes at that time. Further study of the multi-aspect geological characteristics of these coal seams in other parts of the world can establish a more complete evidence chain to uncover the causes of mass extinction.

Author Contributions: Conceptualization, J.W.; methodology, J.W. and X.W.; validation, J.W. and L.S.; writing—original draft preparation, J.W.; writing—review and editing, J.W. and L.S. All authors have read and agreed to the published version of the manuscript.

Funding: This work was supported by the National Natural Science Foundation of China (No. 41602123 and 41572090) and Fundamental Research Funds for the Universities of Henan Province (No. NSFRF 220401).

Data Availability Statement: The raw data supporting the conclusions of this article will be made available by the authors without undue reservation.

Conflicts of Interest: The authors declare that the research was conducted in the absence of any commercial or financial relationships that could be construed as a potential conflicts of interest.

References

1. Benton, M.J.; Newell, A.J. Impacts of global warming on Permo-Triassic terrestrial ecosystems. *Gondwana Res.* **2014**, *25*, 1308–1337. [CrossRef]
2. Shao, L.Y.; Wang, X.T.; Lu, J.; Wang, D.D.; Hou, H.H. A Reappraisal on Development and Prospect of Coal Sedimentology in China. *Acta Sedimentol. Sin.* **2017**, *35*, 1016–1031, (In Chinese with English abstract).
3. Ouyang, S.; Zhu, H.C. Query the assumption of "End-Permian fungal spike event", with special reference to the Permo-Triassic transitional palynofloras. *Acta Palaeontol. Sin.* **2007**, *46*, 394–410, (In Chinese with English abstract).
4. Wu, Y.Y.; Qin, Y.; Wang, A.K.; Shen, J. Geochemical anomaly and the causes of transition metal accumulations in late Permian coal from the eastern Yunnan-western Guizhou region. *Int. J. Min. Sci. Technol.* **2013**, *23*, 105–111. [CrossRef]
5. Williams, M.L.; Jones, B.G.; Carr, P.F. Geochemical consequences of the Permian–Triassic mass extinction in a non-marine succession, Sydney Basin, Australia. *Chem. Geol.* **2012**, *326–327*, 174–188. [CrossRef]
6. Wang, G.Q.; Sun, B.L.; Liu, C.; Wu, J.; Pan, X.Y.; Zeng, F.G. Paleo-peat sedimentary environment and controlling on trace elements: Example from the 11# coal seam in Donglutian Coalmine of Ningwu Coalfield. *J. Palaeogeogr.* **2022**, *24*, 1210–1223, (In Chinese with English abstract).

7. Dai, S.F.; Luo, Y.B.; Seredin, V.V.; Ward, C.R.; Hower, J.C.; Zhao, L.; Liu, S.D.; Zhao, C.L.; Tian, H.M.; Zou, J.H. Revisiting the late Permian coal from the Huayingshan, Sichuan, southwestern China: Enrichment and occurrence modes of minerals and trace elements. *Int. J. Coal Geol.* **2014**, *122*, 110–128. [CrossRef]
8. Oboirien, B.O.; Thulari, V.; North, B.C. Enrichment of trace elements in bottom ash from coal oxy-combustion: Effect of coal types. *Appl. Energy* **2016**, *177*, 81–86. [CrossRef]
9. Fu, X.G.; Wang, J.; Feng, X.L.; Chen, W.B.; Wang, D.; Song, C.Y.; Zeng, S.Q. Mineralogical composition of and trace-element accumulation in lower Toarcian anoxic sediments: A case study from the Bilong Co. oil shale, eastern Tethys. *Geol. Mag.* **2016**, *153*, 618–634. [CrossRef]
10. Diessel, C.F.K. The correlation between coal facies and depositional environments. In *Advances in the Study of the Sydney Basin*; University of Newcastle: Newcastle, Australia, 1986; pp. 19–22.
11. Diessel, C. *Coal-Bearing Depositional Systems*; Thomson Press Ltd.: New Delhi, India, 1992; pp. 161–264.
12. Calder, J.H.; Gibling, M.R.; Mukhopadhyay, P.K. *Peat Formation in a Westphalian B Piedmont Setting, Cumberland Basin, Nova Scotia: Implications for the Maceral-Based Interpretation of Rheotrophic and Raised Paleomires*; Contribution series No. 91-002; Chamber of Mineral Resources of Nova Scotia: Halifax, NS, Canada, 1991; pp. 283–296.
13. Petersen, H.I.; Ratanasthien, B. Coal facies in a Cenozoic paralic lignite bed, Krabi Basin, southern Thailand: Changing peat-forming conditions related to relative sealevel controlled watertable variations. *Int. J. Coal Geol.* **2011**, *87*, 2–12. [CrossRef]
14. Lou, Y.; Su, Y.L.; Wang, W.D.; Xia, P.; Wang, K.; Xiong, W.; Yu, Y.; Shao, L.J.; Yang, F.Q.; Chen, X.P. Coal facies and its effects on pore characteristics of the Late Permian Longtan coal, western Guizhou, China. *Geofluids* **2022**, 6071514. [CrossRef]
15. Kang, S.L. Coal facies model and coal-generated hydrocarbon of the Paleogene to Neogene coals. Ph.D. Thesis, China University of Mining and Technology, Beijing, China, 2021. (In Chinese with English abstract).
16. Moss, P.T.; Greenwood, D.R.; Archibald, S.B. Regional and local vegetation community dynamics of the eocene okanagan highlands (British columbia-Washington state) from palynology. *Can. J. Earth Sci.* **2005**, *42*, 187–204. [CrossRef]
17. Zhao, L.; Ward, C.R.; French, D.; Graham, I.T. Mineralogy of the volcanic-influenced Great Northern coal seam in the Sydney Basin, Australia. *Int. J. Coal Geol.* **2012**, *113*, 94–110. [CrossRef]
18. Finkelman, R.B.; Dai, S.F.; French, D. The importance of minerals in coal as the hosts of chemical elelments: A review. *Int. J. Coal Geol.* **2019**, *212*, 103251. [CrossRef]
19. Shao, L.Y.; Hua, F.H.; Wang, J.; Ji, X.K.; Yan, Z.M.; Zhang, T.C.; Wang, X.T.; Ma, S.M.; Jones, T.; Lu, H.N. Palynological dynamics in the late Permian and the Permian-Triassic transition in southwestern China. *Palaeogeogr. Palaeoclimatol. Palaeoecol.* **2023**, *619*, 111540. [CrossRef]
20. He, B.; Xu, Y.G.; Xiao, L.; Wang, Y.M.; Wang, K.M.; Sha, S.L. Sedimentary Responses to Uplift of Emeishan Mantle Plume and its implications. *Geol. Rev.* **2006**, *52*, 30–37, (In Chinese with English abstract).
21. Wang, Y.; Cao, J.; Zhang, B.L.; Liao, Z.W.; Zhang, B.; Liu, J.C.; Shi, C.H. Genesis of the wangpo bed in the sichuan basin: Formation by eruptions of the emeishan large igneous province. *Palaeogeogr. Palaeoclimatol. Palaeoecol.* **2022**, *594*, 110935. [CrossRef]
22. Bercovici, A.; Cui, Y.; Forel, M.B.; Yu, J.X.; Vajda, V. Terrestrial paleoenvironment characterization across the Permian-Triassic boundary in South China. *J. Asian Earth Sci.* **2015**, *98*, 225–246. [CrossRef]
23. *ASTM Standard D3173-11*; Test Method for Moisture in the Analysis Sample of Coal and Coke. ASTM International: West Conshohocken, PA, USA, 2011.
24. *ASTM Standard D3174-11*; Annual Book of ASTM Standards. Test Method for Ash in the Analysis Sample of Coal and Coke. ASTM International: West Conshohocken, PA, USA, 2011.
25. *ASTM Standard D3175-11*; Test Method for Volatile Matter in the Analysis Sample of Coal and Coke. ASTM International: West Conshohocken, PA, USA, 2011.
26. *Chinese Standard GB/T 40485-2021*; Method of Determining Automatically the Random Reflectance of Vitrinite in Coal-Image Analysis Method. GB Standards: Shenzhen, China, 2021. (in Chinese)
27. *Chinese Standard GB/T 15588-2013*; Classification of Macerals for Bituminous Coal. GB Standards: Shenzhen, China, 2013. (in Chinese)
28. *Chinese Standard GB/T 14506.30-2010*; Methods for Chemical Analysis of Silicate Rocks-Part 30: Determination of 44 Elements. GB Standards: Shenzhen, China, 2010. (in Chinese)
29. *ASTM Standard D388-12*; Standard Classification of Coals by Rank. ASTM International: West Conshohocken, PA, USA, 2012.
30. *Chinese Standard MT/T850-2000*; Classification for Total Moisture in Coal. GB Standards: Shenzhen, China, 2000. (in Chinese)
31. *Chinese Standard GB/T 15224.1-2018*; Classification for Quality of Coal-Part 1: Ash. GB Standards: Shenzhen, China, 2018. (in Chinese)
32. Dai, S.F.; Liu, J.J.; Ward, C.R.; Hower, J.C.; Xie, P.P.; Jiang, Y.F.; Hood, M.M.; O'keefe, J.M.K.; Song, H.J. Petrological, geochemical, and mineralogical compositions of the low-Ge coals from the Shengli Coalfield, China: A comparative study with Ge-rich coals and a formation model for coal-hosted Ge ore deposit. *Ore Geol. Rev.* **2015**, *71*, 318–349. [CrossRef]
33. Ketris, M.P.; Yudovich, Y.E. Estimations of Clarkes for carbonaceous biolithes: World average for trace elements in black shales and coals. *Int. J. Coal Geol.* **2009**, *78*, 135–148. [CrossRef]
34. Wang, J. Geochemistry of Late Permian Coal in Xuanwei, Eastern Yunnan, China and Its Relation to the Permian-Triassic Boundary. Ph.D. Dissertation, Henan Polytechnic University, Jiaozuo, China, 2015.

35. Seredin, V.V.; Dai, S.F. Coal deposits as a potential alternative source for lanthanides and yttrium. *Int. J. Coal Geol.* **2012**, *94*, 67–93. [CrossRef]
36. Dai, S.F.; Ren, D.Y.; Chou, C.L.; Finkelman, R.B.; Seredin, V.V.; Zhou, Y.P. Geochemistry of trace elements in Chinese coals: A review of abundances, genetic types, impacts on human health, and industrial utilization. *Int. J. Coal Geol.* **2012**, *94*, 3–21. [CrossRef]
37. Hao, L.B.; Qi, C.M. *Principles of Geochemistry*; Geological Press: Beijing, China, 2004; pp. 2, 54–55. (In Chinese)
38. Ren, D.Y.; Zhao, F.H.; Dai, S.F.; Zhang, J.Y.; Luo, K.L. *Geochemistry of Trace Elements in Coal*; Science Press: Beijing, China, 2006; pp. 393–401. (In Chinese)
39. Dai, S.F.; Bechtel, A.; Eble, C.F.; Flores, R.M.; French, D.; Graham, I.T.; Hood, M.M.; Hower, J.C.; Korasidis, V.A.; Moore, T.A.; et al. Recognition of peat depositional environments in coal: A review. *Int. J. Coal Geol.* **2020**, *219*, 103383.
40. Tang, X.Y.; Huang, W.H. *Trace Elements of Chinese Coal*; The Commercial Press: Beijing, China, 2004; pp. 3–41. (In Chinese)
41. Qin, G.H.; Cao, D.Y.; Wei, Y.C.; Wang, A.M.; Liu, J.C. Geochemical characteristics of the Permian coals in the Junger-Hebaopian mining district, northeastern Ordos Basin, China: Key role of paleopeatforming environments in Ga-Li-REY enrichment. *J. Geochem. Explor.* **2020**, *213*, 106494. [CrossRef]
42. Roser, B.P.; Korsch, R.J. Determination of tectonic setting of sandstone-mudstone suites using SiO_2 content and K_2O/Na_2O ratio. *J. Geol.* **1986**, *94*, 635–650. [CrossRef]
43. McLennan, S.M.; Hemming, S.; McDaniel, D.K.; Hanson, G.N. Geochemical approaches to sedimentation, provenance, and tectonics. In *Processes Controlling the Composition of Clastic Sediments*; Johnsson, M.J., Basu, A., Eds.; Geological Society of America: Boulder, CO, USA, 1993; pp. 21–40.
44. Kalkreuth, W.D.; Marchioni, D.L.; Calder, J.H.; Lamberson, M.N.; Naylor, R.D.; Paul, J. The relationship between coal petrography and depositional environments from selected coal basins in Canada. *Int. J. Coal Geol.* **1991**, *19*, 21–76. [CrossRef]
45. Thompson, S.; Morley, R.J.; Barnard, P.C.; Cooper, B.S. Facies recognition of some Tertiary coals applied to prediction of oil source rock occurrence. *Mar. Petrol. Geol.* **1985**, *2*, 288–297. [CrossRef]
46. Jiu, B.; Huang, W.H.; Hao, R.L. A method for judging depositional environment of coal reservoir based on coal facies parameters and rare earth element parameters. *J. Pet. Sci. Eng.* **2021**, *207*, 109128. [CrossRef]
47. Liang, H.R.; Xu, G.S.; Yu, Q.; Xu, F.H.; Wang, D.Y.; Chen, Z.Y. Paleosalinity and Its Association with Organic Matter: A Case Study from the Eocene Shahejie Formation, Laizhou Bay Sag, Bohai Bay Basin (China). *J. Ocean Univ. China* **2021**, *20*, 741–754. [CrossRef]
48. Li, J.; Chen, D. Summary of quantified research method on paleosalinity. *Pet. Geol. Recovery Effic.* **2003**, *10*, 1075.
49. Ye, C.C.; Yang, Y.B.; Fang, X.M.; Zhang, W.L. Late Eocene clay boron-derived paleosalinity in the Qaidam Basin and its implications for regional tectonics and climate. *Sediment. Geol.* **2016**, *346*, 49–59. [CrossRef]
50. Zhao, Q.; Wang, J.; Jiang, F.H.; Zhang, C.G. Geochemical characteristics and lake basin evolution of mudstone and shale of the middle section of the third member of Shahejie Formation in Dongpu depression. Mineral. Petrol. 2023. Available online: https://kns.cnki.net/kcms2/detail/51.1143.TD.20230609.0907.002.html (accessed on 10 July 2023). (In Chinese with English abstract).
51. Xiong, X.H.; Xiao, J.F. Geochemical Indicators of Sedimentary Environments—A Summary. *Earth Environ.* **2011**, *39*, 405–414.
52. Hatch, J.R.; Leventhal, J.S. Relationship between inferred redox potential of the depositional environment and geochemistry of the Upper Pennsylvanian (Missourian) Stark Shale Member of the Dennis Limestone, Wabaunsee County, Kansas, USA. *Chem. Geol.* **1992**, *99*, 65–82. [CrossRef]
53. Zarasvandi, A.; Rezaei, M.; Sadeghi, M.; Pourkaseb, H.; Sepahvand, M. Rare-earth element distribution and genesis of manganese ores associated with Tethyan ophiolites, Iran: A review. *Mineral. Mag.* **2016**, *80*, 127–142. [CrossRef]
54. Wallace, M.W.; Hood, A.V.S.; Shuater, A.; Greig APlanavsky, N.J.; Reed, C.P. Oxygenation history of the Neoproterozoic to early Phanerozoic and the rise of land plants. *Earth Planet. Sci. Lett.* **2017**, *466*, 12–19. [CrossRef]
55. Wang, W.F.; Qin, Y.; Song, D.Y.; Fu, X.H. Geochemistry of rare earth elements in the middle and high sulfur coals from North Shanxi Province. *Geochimica* **2002**, *31*, 564–570, (In Chinese with English abstract).